The Impact of Increasing Stratospheric Radiative Damping on the QBO Period

Tiehan Zhou[1,2], Kevin DallaSanta[1,3], Larissa Nazarenko[1,2], Gavin A. Schmidt[1], Zhonghai Jin[1]

[1]NASA Goddard Institute for Space Studies, New York, NY
[2]Center for Climate Systems Research, Columbia University, New York, NY
[3]Universities Space Research Association, Columbia, MD

Correspondence to: Tiehan Zhou (tz2131@columbia.edu)

Abstract. Stratospheric radiative damping increases as atmospheric carbon dioxide concentration rises. We use the one-dimensional mechanistic models of the QBO to conduct sensitivity experiments and find that the simulated QBO period shortens due to the enhancing of radiative damping in the stratosphere. This result suggests that increasing stratospheric radiative damping due to rising CO_2 may play a role in determining the QBO period in a warming climate along with wave momentum flux entering the stratosphere and tropical vertical residual velocity, both of which also respond to increasing CO_2.

Deleted: when atmospheric carbon dioxide concentration increases, …

1. Introduction

The quasi-biennial oscillation (QBO) dominates the variability of the equatorial middle and lower stratosphere and is characterized by a downward propagating zonal wind regime that regularly changes from westerlies to easterlies. The QBO period ranges from 22 to 34 months with its average being slightly longer than 28 months. The QBO not only manifests itself in the equatorial zonal winds, but also leaves an imprint on the temperature in both the tropics and extratropics (Baldwin et al., 2001 and references therein).

The QBO has far-reaching implications for global weather and climate systems. First of all, the QBO exerts a marked influence on the distribution and transport of various chemical constituents such as ozone (O_3) (e.g., Hasebe, 1994), water vapor (H_2O) (e.g., Kawatani et al., 2014), methane (CH_4), nitrous oxide (N_2O), hydrogen fluoride (HF), hydrochloric acid (HC1), odd nitrogen species (NO_y) (e.g., Zawodny and McCormick, 1991), and volcanic aerosol (Trepte and Hitchman, 1992). Secondly, it is well appreciated that the QBO influences the extratropical circulation in the winter stratosphere, which is commonly known as the Holton–Tan effect (Holton and Tan, 1980; Labitzke, 1982). It has been noted that the effect of the QBO on the extratropical winter stratosphere impacts the severity of stratospheric ozone depletion (e.g., Lait et al., 1989). Furthermore, taking account of the QBO improves the simulation and predictability of the extratropical troposphere (e.g., Marshall and Scaife, 2009). Finally, through its modulation of temperature and vertical wind shear in the vicinity of the tropical tropopause, the QBO influences tropical moist convection (Collimore et al., 2003; Liess and Geller, 2012), the El Niño-Southern Oscillation (ENSO) (Gray et al., 1992; Huang et al., 2012; Hansen et al. 2016), the Hadley circulation (Hitchman and Huesmann, 2009), the tropospheric subtropical jet (Garfinkel and Hartmann, 2011a, 2011b), the boreal summer monsoon (Giorgetta et al., 1999), and the Madden-Julian Oscillation (Yoo and Son, 2016**)**. Intriguingly, the QBO is also reported to influence the activities of tropical cyclones (Gray et al., 1984; Ho et al., 2009), albeit this issue is still unsettled (Camargo and Sobel, 2010) and needs further study.

Efforts to understand and simulate the QBO have been ongoing ever since its discovery by Ebdon (1960) and Reed et al. (1961). Lindzen and Holton (1968) and Holton and Lindzen (1972) developed the classical theory of the QBO. Namely, as waves propagate upward, they are attenuated by thermal damping, encounter critical levels, and accelerate and decelerate the mean flow, providing momentum sources for both the westerly and easterly phases of the QBO.

Holton and Lindzen's (1972) model (hereafter referred to as HL model) was further simplified by Plumb (1977), the elegance of which made it a standard paradigm for the QBO. In Plumb's (1977) Boussinesq formulation, the QBO period is inversely dependent upon both the momentum flux and thermal dissipation rate. Hamilton (1981) further highlighted the role of the radiative damping rate on both the realistic vertical structure and the realistic period of the QBO.

By adopting higher vertical resolutions and incorporating various gravity wave parameterization schemes, many state-of-the-art climate models have shown the capability to self-consistently simulate the QBO (Scaife et al., 2000; Giorgetta et al., 2002, 2006; Rind et al., 2014, 2020; Geller et al., 2016a; Richter et al., 2020a, 2020b). Given the important implications of the QBO for the global climate system, it is natural to ask how the QBO will change in a warming climate.

Giorgetta and Doege (2005) showed a shortening of the QBO period in their doubled CO_2 experiments. They reasoned that both the weakening of the tropical upwelling and the prescribed increase of gravity wave sources lead to the reduction of the QBO period in a warming climate. However, most climate models project a strengthening rather than weakening of tropical upwelling in a warmer climate (Butchart et al., 2006; Butchart 2014; Li et al., 2008). Employing a model without any parametrized non-orographic gravity waves, Kawatani et al. (2011) demonstrated that the intensifying tropical upwelling in a warming climate dominates the counteracting effect of enhanced wave fluxes and consequently projected a lengthening of the QBO period. Using fixed sources of parametrized gravity waves, Watanabe and Kawatani (2012) also projected an elongation of the QBO period in a warming climate and ascribed it to the stronger tropical upwelling. Analyzing four Coupled Model Intercomparison Project phase 5 (CMIP5) models that could simulate a reasonable QBO, Kawatani and Hamilton (2013) found that the projected trends of the QBO period were inconsistent in sign. They further investigated the 60-year operational balloon-borne radiosonde observations provided by the Free

Berlin University and detected no significant trend in the QBO period. Richter et al. (2020b) investigated the response of the QBO to doubled and quadrupled CO2 climates among eleven models that participated in Phase 1 of the Stratospheric-tropospheric Processes And their Role in Climate QBO-initiative (QBOi; Butchart et al., 2018), and found no consensus on how the QBO period would respond to a changing climate. Recently, Butchart et al. (2020) evaluated ten Coupled Model Intercomparison Project phase 6 (CMIP6) models with realistic QBO in two Shared Socioeconomic Pathways (SSPs, Gidden et al., 2019) scenario simulations and surprisingly found that the QBO period shortens in seven of those ten models in both in both SSP3-7.0 and SSP5-8.5 scenarios although only two and three models show a significant shortening trend in the respective scenarios.

It is challenging to ascertain the trend of the QBO period in a warming climate. On one hand, a speeding-up of the Brewer-Dobson circulation in a warming climate leads to a lengthening of the QBO period in most climate models. On the other hand, there is a robust increase in the vertical component of the EP flux for both eastward and westward propagating waves (Richter et al., 2020b; Butchart et al., 2020), indicating that the QBO period shortens due to the enhanced wave driving in a warming climate. The competing effects between enhanced wave driving and a faster Brewer-Dobson circulation suggests that trends in the QBO period are likely to be small and difficult to detect due to the large cycle-to-cycle variability that is reproduced by climate models (Butchart et al., 2020). In addition, uncertainty in the representation of the parameterized gravity waves make it more elusive to detect the trend of the QBO period in a warming climate (Schirber et al., 2015; Richter et al., 2020b).

Given the fact that the QBO period is influenced by the radiative damping (Plumb 1977; Hamilton 1981), a natural question to ask is whether it could play a role on the trend of the QBO in a warming climate. Plass (1956) showed that when the CO_2 concentration is increased from 330 ppmv to 660 ppmv, the cooling rate increases significantly in the middle and upper stratosphere while it is not changed below

the 24 km height level. The cooling rate is increased by about 50% around the 40 km height level (see his Figure 8).

It is well-known that enhanced wave fluxes entering the stratosphere and stronger tropical upwelling individually play a dominant role in determining the trends in the QBO period in a warming climate. Does the competing effect between them leave some room for increasing stratospheric radiative damping to exert an influence on the QBO period? In this paper, we use the HL model to isolate the effect of radiative damping on the QBO period by assuming that the momentum flux entering the stratosphere doesn't change in our experiments. Observational and modeling studies (Andrews et al., 1987; Kawatani et al., 2009, 2010, 2011; Richter et al., 2020b; Holt et al., 2020) showed that the wave forcing spectrum is similar to a discrete two-wave spectrum rather than red-noise or white-noise, all of which are illustrated in Saravanan (1990). Accordingly, the QBO is indeed sensitive to stratospheric radiative damping, and the HL model is suitable for us to conduct the sensitivity analysis.

The remainder of this paper is organized as follows. Section 2 investigates the sensitivity of the QBO period to the radiative damping using HL's original model. Section 3 explores the sensitivity of the QBO period to the radiative damping using a modified HL model where the semiannual forcing is removed. Discussion and conclusions are presented in Sections 4 and 5 respectively.

2. Sensitivity of the QBO period to enhanced stratospheric radiative damping in the original HL model

In the HL model the governing equation of mean flow emerges after the primitive momentum equation is meridionally averaged over some suitable latitudinal belt over the equator.

$$\frac{\partial \overline{u}}{\partial t} = -\frac{1}{\rho_0}\frac{\partial}{\partial z}\left[\sum_{i=0}^{1} \overline{F_i}\right] + K_z \frac{\partial^2 \overline{u}}{\partial z^2} + G \qquad (1)$$

where $\overline{u}$ is mean zonal wind, ρ_0 is mean density, $\overline{F_i}$ is the meridionally averaged vertical Eliassen-Palm flux associated with wave i, the index i refers to the individual waves, K_z is a vertical eddy diffusion coefficient, t is time, z is altitude, and G is semiannual forcing identical to that specified by HL.

The $\overline{F_i}$ is are evaluated with Lindzen's (1971) WKB formalism for equatorial waves in shear. When only infrared cooling acts to damp the waves the formulae for $\overline{F_i}$ are

$$\overline{F_0}(z) = A_0\, exp\left(-\int_{17km}^{z} \frac{\alpha N}{k(c-\overline{u})^2}\, dz\right) \tag{2}$$

for the Kelvin wave, and

$$\overline{F_1}(z) = A_1\, exp\left[-\int_{17km}^{z} \frac{\alpha\beta N}{k^3(c-\overline{u})^3}\left(1-\frac{k^2(\overline{u}-c)}{\beta}\right) dz\right] \tag{3}$$

for the mixed Rossby-gravity wave. As in HL, the wavenumber k, the phase speed c, and A_0 are chosen to be $2\pi/(40{,}000\ \text{km})$, $30\ \text{m s}^{-1}$, and $0.04\ \text{m}^2\ \text{s}^{-2}\rho_0(17\ \text{km})$, respectively for the Kelvin wave while they are equal to $-2\pi/(10{,}000\ \text{km})$, $-30\ \text{m s}^{-1}$, and $-0.04\ \text{m}^2\ \text{s}^{-2}\rho_0(17\ \text{km})$, respectively for the mixed Rossby-gravity wave. In Eq. (1), $K_z = 0.3\ \text{m}^2\ \text{s}^{-1}$, which is also the same as in HL. In addition, $\beta = 2\Omega/a$, where Ω is earth's rotation rate, and a is earth's radius. HL's boundary conditions stipulated that $\overline{u} = 0$ at the lowest model level (17 km) and constrained $\overline{u}$ to vary semiannually at the top level (35 km).

In our control run that is used to depict the present-day QBO all the model parameters are identical to those used by HL in their original simulation. The Brunt-Väisälä frequency

$$N = \sqrt{\frac{g}{T_0}\left(\frac{dT_0}{dz} + \frac{g}{c_p}\right)} \tag{4}$$

In Eq. (4), g is gravity, T_0 is mean temperature, and c_p is specific heat of dry air at constant pressure. HL set N in Eq. (4) to $2.16 \times 10^{-2}\text{s}^{-1}$ with a scale height $H = 6\ \text{km}$. In addition, the Newtonian

cooling profile in our control run, i.e., $\alpha(z)$ in Eqs. (2) and (3), is also identical to that in the original HL model and depicted in FIG. 1a as the black line. Namely, $\alpha(z)$ in the control run increases from $(21\ \text{day})^{-1}$ at 17 km to $(7\ \text{day})^{-1}$ at 30 km and is kept at $(7\ \text{day})^{-1}$ between 30 km and 35 km. Fels (1985) explained why the magnitude of this radiative damping rate is suitable for simulating the QBO on the basis of the scale-dependent effect of radiative damping (Fels, 1982). Hamilton (1981) demonstrated that the proper choice of $\alpha(z)$ is crucial in simulating a realistic vertical structure of the QBO.

Deleted: explicated

Deleted: cooling

Eq. (1) was integrated for 100 years using the forward-backward scheme (Matsuno, 1966). The vertical resolution was 250 m and identical to that in HL. The time step was 12 hr, i.e., one half of used in HL, because the 24-hr time step resulted in numerical instability in our integration.

FIG. 2a shows the time–height section of the monthly averaged mean zonal wind simulated over the first 20 years using the HL model. Both the QBO and the semiannual oscillation (SAO) are conspicuous. The fast Fourier transform (FFT) method is used to calculate the frequency power spectra. In order to more accurately derive the QBO period, the model was run for 100 years to increase the spectral resolution. Frequency–height sections of the power spectral densities (PSD) over zero to the Nyquist frequency, i.e., 0.5 cycle/month, depict two sharp lines (peaks) at $\frac{1}{30}$ and $\frac{1}{6}$ cycle/month, respectively (not shown). In order to better visualize the magnitudes of the PSD, we show two truncated frequency–height sections with FIG. 2b and FIG. 2c highlighting the QBO and the SAO respectively. FIG. 2b shows that the QBO dominates over the model domain. The peak frequency corresponds to the period of 30 months. FIG. 2c shows the SAO dominates near the model top due to the fact a semiannual forcing was imposed in the altitudes from 28 to 35 km.

It is worth mentioning that the QBO period shown here is longer than 26.5 months reported in the HL paper (see their FIG. 1). Using the HL model parameters, the QBO period simulated by Plumb (1977)

was close to three years (refer to his FIG. 8a), which is longer than our simulated QBO period, i.e., 30.0 months. Although we could not explain why our simulated QBO period is longer than that simulated by HL, we found that when the upper boundary condition is changed from $\overline{u} = 14 \sin(\omega_a t)$ and $\omega_a = \frac{2\pi}{180}$ day^{-1} used in the HL's original model (refer to their Eqs. (2)) to $\frac{\partial \overline{u}}{\partial z} = 0$ used in Plumb (1977), the simulated QBO period becomes 34.3 month (figure not shown). In other words, when we adopted the stress-free upper boundary condition as in Plumb (1977), our simulated QBO period is comparable to that simulated by him, which lends credence to our reconstruction of the HL model.

As mentioned in Section 1, when the atmospheric carbon dioxide concentration is doubled the cooling rate increases significantly in the middle and upper stratosphere while it varies little below the 24 km height level. Accordingly, $\alpha(z)$ in the experimental run is kept the same as in the control run, i.e, increases from $(21 \text{ day})^{-1}$ at 17 km to $\frac{9}{91}$ day^{-1} at 24 km. Since the cooling rate is increased by about 50% around the 40 km height level (Plass, 1956), the radiative damping rates are expected to also increase in the middle and upper stratosphere as the CO_2 concentration rises. However, the relative change of cooling rate Q in response to the increasing CO_2 is not identical to that of Newtonian cooling coefficient due to the facts that $Q = -\alpha(T - T_e)$ and the radiative equilibrium temperature T_e in the stratosphere decreases as the CO_2 concentrations increase (Manabe et al. 1967). In other words, for any given temperature profile as adopted by Plass (1956), the decreasing of the stratospheric T_e with increasing CO_2 concentration leads to $\alpha_2(z):\alpha_1(z) \neq Q_2(z):Q_1(z)$, where $\alpha_1(z)$and $\alpha_2(z)$ represent the Newtonian cooling coefficient at any altitude z for the reference and doubled CO_2, respectively while $Q_1(z)$ and $Q_2(z)$ stand for the cooling rate likewise. In order to rigorously quantify $\alpha_2(z):\alpha_1(z)$, we follow Dickinson (1973) in using a radiative transfer model to calculate $Q_1(T)$ for a reference temperature profile $T(z)$ and $Q_1(T+\delta)$ for $T_{(z)} + \delta$, where a small perturbation $\delta T = 0.1\ K$ with $T_{(z)}$ being the 1976 U.S. standard atmosphere. Our radiative transfer computations use the MODTRAN

Deleted: does not change

Deleted: The

gas absorption database with 0.1 cm^{-1} spectral resolution (Jin et al. 2019; Berk et al. 2008). We then repeat the computations with the doubled CO_2 to yield $Q_2(T)$ and $Q_2(T+\delta)$. It follows that $\frac{\alpha_2}{\alpha_1} = \frac{Q_2(T+\delta) - Q_2(T)}{Q_1(T+\delta) - Q_1(T)}$. In FIG. 1b the black line depicts the ratio for the broadband longwave radiation ($5\ \mu m - 100\ \mu m$) and the red line delineates the ratio for the CO_2 absorption band ($12\ \mu m - 18\ \mu m$) used by Plass (1956). For the CO_2 absorption band, the calculated ratio is evidently comparable to the ratio of cooling rates between the doubled CO_2 and the reference CO_2 shown in figure 8 of Plass (1956), with an additional small increase (<1.1) below the 24 km level. The ratio calculated over the broadband is conspicuously smaller than that for the CO_2 absorption band, because the changes in cooling rate from the temperature perturbation are larger over a wider spectral band.

Returning to the 1D HL model, we synthesize those findings by prescribing $\alpha_2(z)$ in our experimental runs for the doubled CO_2 as follows: an increase of 30% between 30 and 35 km, no change below 24 km, and linear interpolation between 24 and 30 km. The resulting increase of radiative damping rate from the control runs is depicted as the red line in FIG. 1a. This increase is reasonable based on our results shown in FIG. 1b.

FIG. 3a shows the time–height section of the monthly averaged mean zonal wind simulated over the first 20 years for the doubled CO_2 run, where the increased $\alpha(z)$ depicted as the red line in FIG. 1a was employed while all other parameters are identical to those in the control run. Obviously, the QBO dominates below 28 km while the semiannual oscillation (SAO) dominates above 31 km. Like FIG. 2b and FIG. 2c, we only show two truncated frequency–height sections with FIG. 3b highlighting the QBO and FIG. 3c highlighting the SAO. FIG. 3b also shows that the QBO prevails over the model domain. The peak frequency corresponds to the period of 27.9 months. FIG. 3c shows the SAO dominates near the model top due to the same imposed semiannual forcing as that in the control run.

Deleted: As implied in Dickinson (1973), the estimated cooling coefficient below the 0.2 hPa level is approximately proportional to the estimated cooling rate and is not sensitive to the chosen temperature profile. In other words, the relative increase in the cooling coefficient is roughly equal to the relative increase in the cooling rate as the CO_2 concentration is doubled. Accordingly, the Newtonian cooling profile

Deleted: run

Deleted: ,

Deleted: i.e., $\alpha(z)$ in Eqs. (2) and (3), is specified in FIG. 1 as the red line. Namely, $\alpha(z)$ in the experimental run increases from $(21\ \text{day})^{-1}$ at 17 km to $\frac{9}{91}\text{day}^{-1}$ at 24 km, which is identical to that in the control run from 17 km to 24 km. We increased $\alpha(z)$ in the experimental run between 30 km and 35 km by 30% relative to that in the control run. In other words, $\alpha(z)$ is kept at $\frac{1.3}{7}\text{day}^{-1}$ between 30 km and 35 km in the experimental run. This percentage increase of 30% in $\alpha(z)$ for the doubled CO_2 above 30 km shown in FIG. 1

Deleted: is somewhat less than that implied in the Figure 8 of Plass (1956), because we would like our estimated relative increase in $\alpha(z)$ to err on the conservative side given the inherent uncertainties mentioned by him. Between 24 km and 30 km, $\alpha(z)$ in the experimental run is formulated linearly with height from $\frac{9}{91}\text{day}^{-1}$ at 24 km to at $\frac{1.3}{7}\text{day}^{-1}$ at 30 km.

In summary, using the original HL model we found that the increased radiative damping due to the doubling of CO2 shortens the QBO period by 7% (i.e., decreases from 30 months to 27.9 months).

3. Sensitivity of the QBO period to enhanced stratospheric radiative damping in the modified HL model without the semiannual forcing

HL pointed out that the imposed semiannual oscillation was not essential for their QBO theory. Applying $\frac{\partial \overline{u}}{\partial z} = 0$ as the upper boundary condition, Plumb (1977) showed a simulated QBO without resorting to the semiannual momentum source (refer to his FIG. 8b). In the following control run, all parameters are identical to those used in the previous control run in Section 2 except that G in Eq. (1) is set to zero with $\frac{\partial \overline{u}}{\partial z}$ also being set to zero at $z = 35$ km. Hereafter we refer to it as the Plumb model[1]. FIG. 4a shows the time–height section of the monthly averaged mean zonal wind simulated over the first 20 years using the Plumb model. As expected, the QBO emerges without any trace of SAO since $G = 0$ in Eq. (1). FIG. 4b shows that the QBO dominates over the whole model domain. The peak frequency corresponds to the period of 37.5 months, which is comparable to that simulated by Plumb (1977) shown in his FIG. 8b. Apparently, the QBO period from the Plumb model, i.e., 37.5 months shown in FIG. 4b, is longer than that from the HL model, i.e., 30.0 months shown in FIG. 2b. This is partly because the additional forcing G in Eq. (1) was removed in the Plumb model.

In the following experimental run, all parameters are identical to those used in the previous experimental run in Section 2 except that G in Eq. (1) is set to zero with $\frac{\partial \overline{u}}{\partial z}$ also being set to zero at $z = 35$ km. In other words, the following experimental run using the Plumb model employed the same

[1] Strictly speaking, it is the HL model modified by Plumb (1977). In this paper, we don't use his eponymous model, i.e., the simplest possible model of the QBO, where Boussinesq fluids with uniform mean density were employed, because the HL model and its variant are considerably more realistic.

parameters as the afore-mentioned control run using the Plumb model except that the increased $\alpha(z)$ shown as the red line in FIG. 1a was used in the following experimental run while $\alpha(z)$ shown as the black line in FIG. 1a was used in the above control run. FIG. 5a shows the time–height section of the monthly averaged mean zonal wind simulated over the first 20 years for the doubled CO_2 run. It is natural that only the QBO emerges. A comparison of FIG. 4a and FIG. 5a shows that the QBO period shortens when the infrared damping increases in response to the doubled CO2. FIG. 5b shows that the QBO dominates over the whole model domain. The peak frequency corresponds to the period of 31.6 months.

Using the Plumb model, we found that the increased radiative damping due to the doubling of CO_2 shortens the QBO period by 15.7% (i.e., decreases from 37.5 months to 31.6 months).

4. Discussion

Dunkerton (1997) showed that in the presence of tropical upwelling it was gravity waves rather than large-scale Kelvin and mixed Rossby-gravity waves that contributed the bulk of QBO forcing. Consequently, Geller et al. (2016a, 2016b) pointed out that enough gravity wave momentum flux is required to model the QBO in a self-consistent manner in climate models and that the magnitude of the subgrid-scale gravity wave momentum flux plays a crucial role in determining the QBO period. Since there is no tropical upwelling in either the HL model or the Plumb model, it is natural that planetary-scale Kelvin and mixed Rossby-gravity waves largely determine the QBO periods shown in Sections 2 and 3 due to the fact that the specified G is significantly weaker than that in the terrestrial stratosphere. We conducted another sensitivity test where all parameters are identical to those in the HL model except that G in both the control and experimental runs is twice as large as that used by HL. As the radiative damping profile changes from the black line to the red line above 24 km shown in FIG. 1a, our simulated QBO period decreases from 28.6 months to 27.3 months (figures not shown). This smaller percentage

Deleted: The semiannual forcing, G in Eq. (1), in the HL model is imposed rather than results from the wave-flow interaction. In other words, G in Eq. (1) is independent of mean flow, and is specified as $G = 0$ for $z \leq 28$ km, and $G = \omega_{sa}\overline{u}_{sa}$ for $z > 28$ km ¶
where $\overline{u}_{sa} = 2(z - 28\text{km})$ m s^{-1} km^{-1}sin $(\omega_{sa}t)$ and $\omega_{sa} = \frac{2\pi}{180}$ day^{-1} $\approx 4 \times 10^{-7}$ s^{-1} (refer to Eqs. (2) in HL). Therefore, we have $\frac{\partial^2 \overline{u}_{sa}}{\partial z^2} = 0$ in the HL original model. We furthermore decompose $\overline{u}$ into two components: $\overline{u}_{QBO}$ *and* $\overline{u}_{sa}$. Combining Eq. (1), the decomposition of $\overline{u}$ *as* $\overline{u} = \overline{u}_{QBO} + \overline{u}_{sa}$, the above-mentioned $\frac{\partial^2 \overline{u}_{sa}}{\partial z^2} = 0$, and $G = \omega_{sa}\overline{u}_{sa} = \frac{\partial \overline{u}_{sa}}{\partial t}$ for $z > 28$ km, yields¶
$$\frac{\partial \overline{u}_{QBO}}{\partial t} = -\frac{1}{\rho_0}\frac{\partial}{\partial z}\left[\sum_{i=0}^{1}\overline{F_i}\right] + K_z\frac{\partial^2 \overline{u}_{QBO}}{\partial z^2} \quad (5)$$¶
for $z > 28$ km.¶

Deleted: and the semiannual forcing, G, is dependent on neither $\overline{u}$ in Eq. (1) nor $\overline{u}_{QBO}$ in Eq. (5),

Deleted: only exerts

Deleted: a

Deleted: weak

Deleted: influence on the planetary wave forcing, i.e., $-\frac{1}{\rho_0}\frac{\partial}{\partial z}\left[\sum_{i=0}^{1}\overline{F_i}\right]$ in Eqs. (1) and (5)

339 decrease of 4.5% is not unexpected because G is not sensitive to the radiative damping at all and the
340 greater specified G reduces the fraction of the total wave forcing arising from the planetary waves.
341 We further conducted two sensitivity tests where all parameters are identical to those in the HL model
342 except that G in the first test is half as large as that used by HL and is equal to zero in the second test.
343 Surprisingly, as the radiative damping profile changes from the black line to the red line above 24 km
344 shown in FIG. 1a, our simulated QBO periods decreases from 30.0 months to 28.6 months both for G
345 being decreased by 50% and for $G = 0$ (figures not shown). This 4.7% decrease in the QBO period is
346 smaller than the 7% reduction obtained from the sensitivity test presented in Section 2 when G is the
347 same as that used by HL. It is surprising because the model atmosphere is expected to be more sensitive
348 to the changes in the radiative damping as G becomes smaller and smaller. Note that when our control
349 runs adopt the black radiative damping profile shown in FIG. 1a the simulated QBO periods are not
350 sensitive to the imposed semiannual forcing provided that G does not exceed the values employed by
351 HL. Similarly, when our experimental runs adopt the red radiative damping profile above 24 km shown
352 in FIG. 1a the simulated QBO periods are also not sensitive to the imposed semiannual forcing provided
353 that G does not exceed 50% of the values adopted in HL. The question naturally arises: what is
354 responsible for this unexpected behavior?
355 In Section 2, the simulated QBO periods are equal to 30 and 34.3 months when we adopted the no-
356 slip and stress-free upper boundary condition respectively with all other parameters being identical to
357 those used by HL. The results implicate the upper boundary conditions in the inconsistency. Plumb (1977)
358 pointed out that the upper boundary in HL was undesirably low and implied that raising the lid to an
359 additional 50% would be adequate for the robustness in his model. Here, we carry out a series of
360 sensitivity tests by raising the model lid gradually from 35 km to 55 km with the one-kilometer increment.
361 we will demonstrate how the behavior of the HL model with $G = 0$ converges with that of the Plumb

Deleted: the unrealistically larger

Deleted: that

Deleted: independent of $\overline{u}$

Deleted: makes

Deleted: the model atmosphere less sensitive to the changes in the radiative damping

Deleted: somewhat

Deleted: unphysical

model. The modified HL model, i.e., the HL model with $G = 0$ is identical to the Plumb model except that the former has the no-slip upper boundary condition while the latter has the stress-free upper boundary condition. Both models share the same governing equation (5). Note that we set the radiative damping rate above the 35 km level to its value at the 35 km level shown in FIG. 1a.

For the radiative damping profile corresponding to the reference CO_2, FIG. 6 shows that when the model lid is placed at the 35 km level the simulated QBO period of 30.0 months with the no-slip upper boundary condition (solid black line) is apparently shorter than that of 37.5 months with the stress-free upper boundary condition (dashed black line). FIG. 6 also shows that as the model lid is raised incrementally from the 35 km level to the 46 km level, the discrepancies between the simulated QBO periods due to the different upper boundary conditions decrease monotonically. No matter whether we adopt the no-slip or stress-free upper boundary condition, the simulated QBO period is 32.4 months for the reference radiative damping profile provided that the model top is at or above the 46 km level.

Similarly, for the radiative damping profile corresponding to the doubled CO_2, FIG. 6 demonstrates that when the model lid is placed at the 35 km level the simulated QBO period of 28.6 months with the no-slip upper boundary condition (solid red line) is obviously shorter than that of 31.6 months with the stress-free upper boundary condition (dashed red line). FIG. 6 also exhibits that as the model lid is raised gradually from the 35 km level to the 40 km level, the discrepancies between the simulated QBO periods due to the different upper boundary conditions decrease monotonically. No matter whether we adopt the no-slip or stress-free upper boundary condition, the simulated QBO period for the enhanced infrared cooling due to the doubled CO_2 is 30.0 months provided that the model top is at or above the 40 km level. It is apparent that the required model top is lower when the radiative damping is augmented due to the doubling of CO_2 because the planetary waves dissipate more steeply with height in presence of the enhanced infrared cooling rates.

FIG. 6 suggests that when the model lid is sufficiently high the QBO period in response to the enhanced radiative damping due to the increasing CO_2 will decrease from 32.4 to 30.0 months. This 7.4% decrease in the QBO period is independent of the upper boundary condition. Plass (1956) indicated that the probable error of the cooling rate was about 10% below 20 km, increasing to 30% at 50 km and that the relative differences between the cooling rates should be considerably more accurate than their magnitude. In other words, the relative differences between the various cooling rates calculated by Plass (1956) should be considerably smaller 30%. Using the HL model with its top at the 48 km level, we further conducted two experiments by adopting $G = 0$ in Eq. (1) and increasing the radiative damping corresponding to the doubled CO_2 between 30 km and 48 km by $30\% - 30\% * 30\% = 21\%$ and $30\% + 30\% * 30\% = 39\%$ respectively relative to that in the control run. The simulated QBO periods are 30.8 and 29.3 months respectively. Therefore, when the model lid is sufficiently high the QBO period in response to the enhanced radiative damping due to the doubled CO_2 will decrease by approximately $7.4\% \pm 2.5\%$.

Jonsson et al. (2004) showed that the doubled CO_2 induces a substantial cooling throughout most of the middle atmosphere, which in turn increases the ozone mixing ratio by 15–20% in the upper stratosphere and by 10–15% in the lower mesosphere (refer to their Figure 6). Incorporating this increase into the ozone profile for the doubled CO_2, we recalculated the ratio of α_2, the Newtonian cooling coefficient for the doubled CO_2, to α_1, the Newtonian cooling coefficient for the reference CO_2. Our calculated α_2/α_1 is only slightly increased as compared with that shown FIG. 1b no matter whether the CO_2 absorption band is $5\ \mu m - 100\ \mu m$ or $12\ \mu m - 18\ \mu m$ (figure not shown). It is not unexpected because the infrared radiative cooling by ozone is significantly smaller than that by CO_2 (refer to Fig. 1 in Dickinson 1973) and, as a result, the 15–20% increases in the ozone mixing ratio will not make a

noticeable difference. Consequently, the QBO period is expected to be marginally influenced by the change in the radiative damping due to the increase in ozone in response to the doubled CO_2.

Note that N, the Brunt-Väisälä frequency, in Eqs. (2) and (3) also changes with increasing CO_2. Richter et al. (2020b) showed that N^2 would be decreased by $\sim 5\%$ in the stratosphere when CO_2 is doubled (refer to their Figure 2c). We used the HL model to conduct a sensitivity test by adopting $G = 0$ in Eq. (1) with the radiative damping profile corresponding to the doubled CO_2 and the top of the models at the 48 km level. The rest of parameters in this sensitivity test are identical to those in all the previous runs except that the Brunt-Väisälä frequency in this experimental run was 2.5% smaller than that in the control run. The models were run for 1000 years to further increase the spectral resolution. We found that when the Brunt-Väisälä frequency was decreased by 2.5%, the simulated QBO period was slightly lengthened from 30 months to 30.2 months (figure not shown). In other words, the impact of decreasing stratospheric buoyancy frequency on the QBO period is almost negligible.

Analyzing eleven CCMI-1 REF-C2 climate–chemistry simulations, Eichinger and Šácha (2020) showed that the scale height in the stratosphere decreases by 2.3% per century. Accordingly, we used the HL model to conduct another sensitivity test by adopting $G = 0$ in Eq. (1) with the radiative damping profile corresponding to the doubled CO_2 and the top of the models at the 48 km level. The rest of parameters in this sensitivity test are identical to those in all the previous control runs except that the scale height in this experimental run was 2.3% smaller than that in the control run. The model was also run for 1000 years for the sake of higher spectral resolution. We found that when the scale height was decreased by 2.3%, the simulated QBO period was also shortened by about 2.3%, i.e., from 30 months to 29.3 months (figure not shown). Apparently, the shortening of the QBO period due to the warming climate is ascribed less to the shrinkage of the scale height in the stratosphere than to the enhancing of

the stratospheric radiative damping. Together, the shrinking scale height and the increasing radiative damping shorten the QBO period by about 9.6%.

5. Conclusions

Plumb (1977) envisioned that stratospheric climate change would give rise to long-term changes in the QBO period due to changes in radiative damping and the Brunt-Väisälä frequency. Using one-dimensional (1D) models and taking into account the uncertainty due to the radiative damping rate, we found that the enhanced radiative damping arising from the doubling of CO2 leads to the shortening of the QBO period by about $7.4\% \pm 2.5\%$ provided that the model top is higher than the 46 km level. Furthermore, when we incorporated both the 2.3% shrinkage of the scale height and the enhanced radiative damping, the QBO period is shortened by about 9.6%. In addition, the impact of decreasing stratospheric buoyancy frequency and increasing radiative damping due to the increased ozone on the QBO period is marginal. Note that those models include neither gravity waves nor tropical upwelling and assume that there are no changes in wave fluxes entering the equatorial stratosphere.

From a comprehensive model perspective, Richter et al. (2020b) showed that the changes in period of the QBO in warming climate simulations varied quite significantly among these models. Some models projected longer mean periods and some shorter mean periods for the QBO in a future warmer climate. They argue that uncertainty in the representation of the parameterized gravity waves is the most likely cause of the spread among the QBOi models in the QBO's response to climate change.

In addition, CO2 increases in the NASA Goddard Institute for Space Studies Model E2.2-AP (Rind et al. 2020; Orbe et al. 2020) lead to a decrease of both QBO period and QBO amplitude (DallaSanta et al., 2021). The period decrease is associated with increases in lower stratospheric momentum fluxes (related to parameterized convection), a finding consistent with Geller et al. (2016a, 2016b) and Richter

et al. (2020b). The amplitude decrease is associated with a strengthened residual mean circulation, also consistent with the literature, although the vertical structure of the circulation response is nontrivial. It is worth mentioning that horizontal momentum flux divergences could also play an important role in weakening the QBO (Match and Fueglistaler, 2019, 2020).

Our 1D models only explored how the QBO period responds to the enhancing radiative damping of planetary waves, the shrinking scale height in the stratosphere, and the decreasing stratospheric buoyancy frequency due to the increasing CO_2 concentration. In order to investigate how those factors affect gravity waves which play an even more important role in determining the QBO period than planetary waves, high-resolution models such as those used by Kawatani et al. (2011, 2019) are desirable to further our understanding. Ultimately, how the QBO period changes in response to the increasing CO_2 will be determined by the combined effects of the strengthening of tropical upwelling, the increasing of wave fluxes entering the equatorial stratosphere, the enhancing of radiative damping, and the shrinking of the scale height in the stratosphere, which warrants further research.

Data availability

Any data used in this paper can be made available from the corresponding author upon request.

Author contributions

All authors made equal contributions to this work.

Competing interests

The authors declare that they have no conflict of interest.

Acknowledgements: Climate modeling at GISS is supported by the NASA Modeling, Analysis and Prediction program, and resources supporting this work were provided by the NASA High-End Computing (HEC) Program through the NASA Center for Climate Simulation (NCCS) at Goddard Space Flight Center. KD acknowledges support from the NASA Postdoctoral Program. The authors thank the editor Peter Haynes and two anonymous reviewers for their helpful comments, which led to an improved paper. The authors also acknowledge very useful discussions with Drs. Geller and Orbe.

References

Andrews, D. G., Holton, J. R., and Leovy, C. B.: Middle Atmosphere Dynamics, Academic Press, 489 pp, 1987.

Baldwin, M. P., Gray, L. J., Dunkerton, T. J., Hamilton, K., Haynes, P. H., Randel, W. J., Holton, J. R., Alexander, M. J., Hirota, I., Horinouchi, T., Jones, D. B. A., Kinnersley, J. S., Marquardt, C., Sato, K., and Takahashi, M.: The Quasi-biennial oscillation, Rev. Geophys., 39, 179–229, https://doi.org/10.1029/1999RG000073, 2001.

Berk, A., Anderson, G. P., Acharya, P. K., Shettle, E. P.: MODTRAN5 version 2 user's manual, Spectral Sciences, Inc., Burlington MA and Air force Geophysics Laboratory, Hanscom AFB, MA, 2008.

Butchart, N.: The Brewer-Dobson circulation, Rev. Geophys., 52, 157–184, https://doi.org/10.1002/2013RG000448, 2014.

Butchart, N., Scaife, A. A., Bourqui, M., Grandpré, J., Hare, S. H., Kettleborough, J., Langematz, U., Manzini, E., Sassi, F., Shibata, K., Shindell, D. and Sigmond, M.: Simulations of anthropogenic change in the strength of the Brewer–Dobson circulation, Climate Dynamics, 27, 727–741, https://doi.org/10.1007/s00382-006-0162-4, 2006.

Butchart, N., Anstey, J., Hamilton, K., Osprey, S., McLandress, C., Bushell, A. C., Kawatani, Y., Kim, Y.-H., Lott, F., Scinocca, J., Stockdale, T.N., Andrews, M., Bellprat, O., Braesicke, P., Cagnazzo, C., Chen, C.-C., Chun, H.-Y., Dobrynin, M., Garcia, R., Garcia-Serrano, J., Gray, L.J., Holt, L., Kerzenmacher, T., Naoe, H., Pohlmann, H., Richter, J. H., Scaife, A.A., Schenzinger, V., Serva, F., Versick, S., Watanabe, S., Yoshida, K. and Yukimoto, S.: Overview of experiment design and comparison of models participating in phase 1 of the SPARC Quasi-Biennial Oscillation initiative (QBOi), Geoscientific Model Development, 11, 1009–1032. https://doi.org/10.5194/gmd-11-1009-2018, 2018.

Butchart, N., Anstey, J. A., Kawatani, Y., Osprey, S. M., Richter, J. H., Wu, T.: QBO changes in CMIP6 climate projections, *Geophys. Res. Lett.,* 47, 1–10. https://doi.org/10.1029/2019GL086903, 2020.

Camargo, S. J. and Sobel, A. H.: Revisiting the influence of the quasi-biennial oscillation on tropical cyclone activity, J. Climate, 23, 5810–5825, https://doi.org/10.1175%2F2010JCLI3575.1, 2010.

Collimore, C. C., Martin, D. W., Hitchman, M. H., Huesmann, A., and Waliser, D. E.: On the relationship between the QBO and tropical deep convection, J. Climate, 16, 2552–2568, https://doi.org/10.1175/1520-0442(2003)016%3C2552:OTRBTQ%3E2.0.CO;2, 2003.

DallaSanta, K., Orbe, C., Rind, D., Nazarenko, L., and Jonas, J.: Dynamical and trace gas responses of the Quasi-Biennial Oscillation to increased CO_2, J. Geophys. Res. Atmos., 126, e2020JD034151. https://doi.org/10.1029/2020JD034151, 2021.

Dickinson, R. E.: Method of parameterization for infrared cooling between altitudes of 30 and 70 kilometers, J. Geophys. Res., 78, 4451–4457, https://doi.org/10.1029/JC078i021p04451, 1973.

Dunkerton, T. J.: The role of gravity waves in the quasi-biennial oscillation, J. Geophys. Res., 102, 26053–26076, https://doi.org/10.1029/96JD02999, 1997.

Ebdon, R. A.: Notes on the wind flow at 50 mb in tropical and subtropical regions in January 1957 and in 1958, Q. J. Roy. Meteor. Soc., 86, 540–542, https://doi.org/10.1002/qj.49708637011, 1960.

Eichinger, R. and Šácha, P.: Overestimated acceleration of the advective Brewer-Dobson circulation due to stratospheric cooling, Q. J. R. Meteorol. Soc., 1-15, https://doi.org/10.1002/qj.3876, 2020.

Fels, S. B.: A parameterization of scale-dependent radiative damping rates in the middle atmosphere, J. Atmos. Sci., 39, 1141–1152, https://doi.org/10.1175/1520-0469(1982)039%3C1141:APOSDR%3E2.0.CO;2, 1982.

Fels, S. B.: Radiative-dynamical interactions in the middle atmosphere, Advances in Geophysics, Vol. 28A, Academic Press, 277–300, https://doi.org/10.1016/S0065-2687(08)60227-7, 1985.

Garfinkel, C. I. and Hartmann, D. L.: The influence of the quasi-biennial oscillation on the troposphere in winter in a hierarchy of models. Part I: Simplified dry GCMs, J. Atmos. Sci., 68, 1273–1289, https://doi.org/10.1175%2F2011JAS3665.1, 2011a.

Garfinkel, C. I. and Hartmann, D. L.: The influence of the quasi-biennial oscillation on the troposphere in winter in a hierarchy of models. Part II: Perpetual winter WACCM runs, J. Atmos. Sci., 68, 2026–2041, https://doi.org/10.1175%2F2011JAS3702.1, 2011b.

Geller, M. A., Zhou, T., Shindell, D., Ruedy, R., Aleinov, I., Nazarenko, L., Tausnev, N. L., Kelley, M., Sun, S., Cheng, Y., Field, R. D., and Faluvegi, G.: Modeling the QBO-improvements resulting from higher-model vertical resolution, J. Adv. Model. Earth Syst., 8, 1092–1105, https://doi.org/10.1002/2016MS000699, 2016a.

Geller, M. A., Zhou, T., and Yuan, W.: The QBO, gravity waves forced by tropical convection, and ENSO, J. Geophys. Res. Atmos., 121, 8886-8895, https://doi.org/10.1002/2015JD024125, 2016b.

Gidden, M. J., Riahi, K., Smith, S. J., Fujimori, S., Luderer, G., Kriegler, E., van Vuuren, D. P., van den Berg, M., Feng, L., Klein, D., Calvin, K., Doelman, J. C., Frank, S., Fricko, O., Harmsen, M.,

Hasegawa, T., Havlik, P., Hilaire, J., Hoesly, R., Horing, J., Popp, A., Stehfest, E., and Takahashi, K.: Global emissions pathways under different socioeconomic scenarios for use in CMIP6: a dataset of harmonized emissions trajectories through the end of the century, Geosci. Model Dev., 12, 1443–1475, https://doi.org/10.5194/gmd-12-1443-2019, 2019.

Giorgetta, M. A. and Doege, M. C.: Sensitivity of the Quasi-Biennial Oscillation to CO_2 doubling, Geophys. Res. Lett., 32, L08701. https://doi.org/10.1029/2004GL021971, 2005.

Giorgetta, M. A., Bengtson, L., and Arpe, K.: An investigation of QBO signals in the east Asian and Indian monsoon in GCM experiments, Climate Dynamics, 15, 435–450, https://doi.org/10.1007/s003820050292, 1999.

Giorgetta, M. A., Manzini, E., and Roeckner, E.: Forcing of the quasi-biennial oscillation from a broad spectrum of atmospheric waves, *Geophys. Res. Lett.*, 29, https://doi.org/10.1029/2002GL014756, 2002.

Giorgetta, M. A., Manzini, E., and Roeckner, E., Esch, M., and Bengtsson, L.: Climatology and forcing of the quasi-biennial oscillation in the MAECHEM5 model, J. Climate, 19, 3882–3901, https://doi.org/10.1175/JCLI3830.1, 2006.

Gray, W. M.: Atlantic seasonal hurricane frequency. Part I: El Niño and 30-mb quasi-biennial oscillation influences, Mon. Wea. Rev., 112, 1649–1688, https://doi.org/10.1175/1520-0493(1984)112%3C1649:ASHFPI%3E2.0.CO;2, 1984.

Gray, W. M., Sheaffer, J. D., and Knaff, J.: Influence of the stratospheric QBO on ENSO variability, J. Meteor. Soc. Jpn., 70, 975–995, https://doi.org/10.2151/jmsj1965.70.5_975, 1992.

Hamilton, K.: The vertical structure of the quasi-biennial oscillation: Observations and theory, Atmos. Ocean, 19, 236–250, http://dx.doi.org/10.1080/07055900.1981.9649111, 1981.

572 Hansen, F., Matthes, K., and Wahl, S.: Tropospheric QBO–ENSO interactions and differences between
573 the Atlantic and Pacific, J. Climate, 29, 1353–1368, https://doi.org/10.1175/JCLI-D-15-0164.1,
574 2016
575 Hasebe, F.: Quasi-biennial oscillations of ozone and diabatic circulation in the equatorial stratosphere, J.
576 Atmos. Sci., 51, 729–745, https://doi.org/10.1175/1520-
577 0469(1994)051%3c0729:QBOOOA%3e2.0.CO;2, 1994.
578 Hitchman, M. H., and Huesmann, A. S.: Seasonal influence of the quasi-biennial oscillation on
579 stratospheric jets and Rossby wave breaking, J. Atmos. Sci., 66, 935–946,
580 https://doi.org/10.1175%2F2008JAS2631.1, 2009.
581 Ho, C.-H., Kim, H.-S., Jeong, J.-H., and Son, S.-W.: Influence of stratospheric quasi-biennial oscillation
582 on tropical cyclone tracks in the western North Pacific, Geophys. Res. Lett., 36, L06702,
583 http://dx.doi.org/10.1029/2009GL037163, 2009.
584 Holt, L., Lott, F., Garcia, R., Kiladis, G.N., Anstey, J.A., Braesicke, P., Bushell, A.C., Butchart, N.,
585 Cagnazzo, C., Chen, C.-C., Chun, H.-Y., Hamilton, K., Kawatani, Y., Kerzenmacher, T., Kim, Y.-
586 H., McLandress, C., Naoe, H., Osprey, S., Richter, J.H., Scinocca, J., Serva, F., Versick, S.,
587 Watanabe, S., Yoshida, K., and Yukimoto, S.: An evaluation of tropical waves and wave forcing of
588 the QBO in the QBOi models, Q. J. R. Meteorol. Soc., https://doi.org/10.1002/qj.3827, 2020.
589 Holton, J. R. and Lindzen, R. S.: An updated theory for the quasi-biennial cycle of the tropical
590 stratosphere, J. Atmos. Sci., 29, 1076–1080, https://doi.org/10.1175/1520-
591 0469(1972)029%3c1076:AUTFTQ%3e2.0.CO;2, 1972.
592 Holton, J. R. and Tan, H.: The Influence of the equatorial quasi-biennial oscillation on the global
593 circulation at 50 mb, J. Atmos. Sci., 37, 2200–2208, https://doi.org/10.1175/1520-
594 0469(1980)037%3c2200:TIOTEQ%3e2.0.CO;2, 1980.

595 Huang, B. H., Hu, Z. Z., Kinter, J. L., Wu, Z. H., and Kumar, A.: Connection of stratospheric QBO with
596 global atmospheric general circulation and tropical SST. Part I: Methodology and composite life
597 cycle, Climate Dynamics, 38, 1–23, https://doi.org/10.1007%2Fs00382-011-1250-7, 2012.
598 Jin, Z., Zhang, Y.-C., Del Genio, A., Schmidt, G., and Kelley, M.: Cloud scattering impact on thermal
599 radiative transfer and global longwave radiation, J. Quant. Spectrosc. Radiat. Transfer, 239, 106669,
600 https://doi.org/10.1016/j.jqsrt.2019.106669, 2019.
601 Jonsson, A., de Grandpre, J., Fomichev, V., McConnell, J., and Beagley, S.: Doubled CO2-induced
602 cooling in the middle atmosphere: Photochemical analysis of the ozone radiative feedback, J.
603 Geophys. Res., 109, D24103, https://doi.org/10.1029/2004JD005093, 2004.
604 Kawatani, Y. and Hamilton, K.: Weakened stratospheric Quasi-Biennial Oscillation driven by increased
605 tropical mean upwelling, Nature, 497, 478–481, https://doi.org/10.1038/nature12140, 2013.
606 Kawatani, Y., Takahashi, M., Sato, K., Alexander, S. P., and Tsuda, T.: Global distribution of
607 atmospheric waves in the equatorial upper troposphere and lower stratosphere: AGCM simulation
608 of sources and propagation, J. Geophys. Res., 114, D01102, https://doi.org/10.1029/2008JD010374,
609 2009.
610 Kawatani, Y., Watanabe, S., Sato, K., Dunkerton, T. J., Miyahara, S., and Takahashi, M.: The roles of
611 equatorial trapped waves and internal inertia-gravity waves in driving the Quasi-Biennial oscillation.
612 Part I: Zonal mean wave forcing, J. Atmos. Sci., 67, 963–980,
613 https://doi.org/10.1175/2009JAS3222.1, 2010.
614 Kawatani, Y., Hamilton, K., and Watanabe, S.: The quasi-biennial oscillation in a double CO2 climate,
615 J. Atmos. Sci., 68, 265–283, https://doi.org/10.1175/2010JAS3623.1, 2011.

Kawatani, Y, Lee, J. N., and Hamilton, K.: Interannual variations of stratospheric water vapor in MLS observations and climate model simulations, J. Atmos. Sci., 71, 4072–4085, https://doi.org/10.1175/JAS-D-14-0164.1, 2014.

Kawatani, Y., Hamilton, K., Sato, K., Dunkerton, T. J., Watanabe, S., and Kikuchi, K.: ENSO Modulation of the QBO: Results from MIROC Models with and without Nonorographic Gravity Wave Parameterization, J. Atmos. Sci., 76, 3893–3917, https://doi.org/10.1175/JAS-D-19-0163.1, 2019.

Labitzke, K.: On the interannual variability of the middle stratosphere during the northern winters, J. Meteorol. Soc. Jpn., 80, 963–971, http://doi.org/10.2151/jmsj1965.60.1_124, 1982.

Lait, L. R., Schoeberl, M. R., and Newman, P. A.: Quasi-biennial modulation of the Antarctic ozone depletion, J. Geophys. Res., 94, 11559–11571, http://dx.doi.org/10.1029/JD094iD09p11559, 1989.

Li, F., Austin, J., and Wilson, R. J.: The strength of the Brewer–Dobson circulation in a changing climate: Coupled chemistry–climate model simulations, J. Climate, 21, 40–57, https://doi.org/10.1175/2007JCLI1663.1, 2008.

Liess, S. and Geller, M. A.: On the relationship between QBO and distribution of tropical deep convection, J. Geophys. Res., 117, D03108, http://dx.doi.org/10.1029/2011JD016317, 2012.

Lindzen, R. S.: Equatorial planetary waves in shear: Part I, J. Atmos. Sci. 28, 609-622, https://doi.org/10.1175/1520-0469(1971)028%3C0609:EPWISP%3E2.0.CO;2, 1971.

Lindzen, R. S. and Holton, J. R.: A theory of the quasi-biennial oscillation, J. Atmos. Sci., 25, 1095–1107, https://doi.org/10.1175/1520-0469(1968)025%3C1095:ATOTQB%3E2.0.CO;2, 1968.

Manabe, S. and Wetherald, R. T.: Thermal equilibrium of the atmosphere with a given distribution of relative humidity, J. Atmos. Sci., 24, 241–259, https://doi.org/10.1175/1520-0469(1967)024%3C0241:TEOTAW%3E2.0.CO;2, 1967.

638 Marshall, A. G. and Scaife, A. A.: Impact of the QBO on surface winter climate, J. Geophys. Res., 114,
639 D18110, http://dx.doi.org/10.1029/2009JD011737, 2009.
640 Match, A., and Fueglistaler, S.: The buffer zone of the quasi-biennial oscillation, J. Atmos. Sci., 76, 3553–
641 3567, https://doi.org/10.1175/JAS-D-19-0151.1, 2019
642 Match, A., and Fueglistaler, S.: Mean-flow damping forms the buffer zone of the quasi-biennial
643 oscillation: 1D theory. J. Atmos. Sci., 77, 1955–1967, https://doi.org/10.1175/JAS-D-19-0293.1,
644 2020.
645 Matsuno, T.: Numerical integrations of primitive equations by use of a simulated backward difference
646 method, J. Meteor. Soc. Japan, 44, 76–84, https://doi.org/10.2151/jmsj1965.44.1_76, 1966.
647 Orbe, C., Rind, D., Jonas, J., Nazarenko, L., Faluvegi, G., Murray, L.T., Shindell, D.T., Tsigaridis, K.,
648 Zhou, T., Kelley, M., and Schmidt, G.: GISS Model E2.2: A climate model optimized for the middle
649 atmosphere. Part 2: Validation of large-scale transport and evaluation of climate response. *J.*
650 *Geophys. Res. Atmos.*, 125, e2020JD033151, https://doi.org/10.1029/2020JD033151, 2020.
651 Plass, G. N.: The influence of the 15μ carbon-dioxide band on the atmospheric infra-red cooling rate,
652 Quart. J. Roy. Meteor. Soc., 82, 310–324, https://doi.org/10.1002/qj.49708235307, 1956.
653 Plumb, R. A.: The interaction of two internal waves with the mean flow: Implications for the theory of
654 the quasi-biennial oscillation, J. Atmos. Sci., 34, 1847–1858, https://doi.org/10.1175/1520-
655 0469(1977)034<1847:TIOTIW>2.0.CO;2, 1977.
656 Reed, R. J., Campbell, W. J., Rasmussen, L. A., and Rogers, D. G.: Evidence of a downward-propagating,
657 annual wind reversal in the equatorial stratosphere, J. Geophys. Res., 66, 813–818,
658 http://dx.doi.org/10.1029/JZ066i003p00813, 1961.

Richter, J. H., Anstey, J. A., Butchart, N., Kawatani, Y., Meehl, G. A., Osprey, S., & Simpson, I. R., 2020b: Progress in simulating the quasi-biennial oscillation in CMIP models. Journal Geophysical Research: Atmospheres, 125, e2019JD032362, https://doi.org/10.1029/2019JD032362, 2020a.

Richter, J. H., Butchart, N., Kawatani, Y., Bushell, A. C., Holt, L., Serva, F., Anstey, J., Simpson, I. R., Osprey, S., Hamilton, K., Braesicke, P., Cagnazzo, C., Chen, C.-C., Garcia, R. R., Gray, L. J., Kerzenmacher, T., Lott, F., McLandress, C., Naoe, H., Scinocca, J., Stockdale, T. N, Versick, S., Watanabe, S., Yoshida, K., Yukimoto, S.: Response of the Quasi-Biennial Oscillation to a warming climate in global climate models, Q. J. R. Meteorol. Soc., 1–29. https://doi.org/10.1002/qj.3749, 2020b.

Rind, D., Jonas, J., Balachandran, N., Schmidt, G., and Lean, J.: The QBO in two GISS global climate models: 1. Generation of the QBO, J. Geophys. Res. Atmos., 119, 8798–8824, https://doi.org/10.1002/2014JD021678, 2014.

Rind, D., Orbe, C., Jonas, J., Nazarenko, L., Zhou, T., Kelley, M., Lacis, A., Shindell, D., Faluvegi, Russell, G., Bauer, M., Schmidt, G., Romanou, A., and Tausnev, N.: GISS Model E2.2: A climate model optimized for the middle atmosphere — Model structure, climatology, variability and climate sensitivity, J. Geophys. Res. Atmos., 125, e2019JD032204, https://doi.org/10.1029/2019JD032204, 2020.

Saravanan, R.: A multiwave model of the quasi-biennial oscillation, J. Atmos. Sci., 47, 2465–2474, https://doi.org/10.1175/1520-0469(1990)047%3C2465:AMMOTQ%3E2.0.CO;2, 1990.

Scaife, A. A., Butchart, N., Warner, C. D., Stainforth, D., Norton, W., and Austin, J.: Realistic quasi-biennial oscillations in a simulation of the global climate, Geophys. Res. Lett., 27, 3481–3484, https://doi.org/10.1029/2000GL011625, 2000.

Schirber, S., Manzini, E., Krismer, T. and Giorgetta, M.: The Quasi-Biennial Oscillation in a warmer climate: sensitivity to different gravity wave parameterizations, Climate Dynamics, 45, 825–836, https://doi.org/10.1007/s00382-014-2314-2, 2015.

Trepte, C. R. and Hitchman, M. H.: Tropical stratospheric circulation deduced from satellite aerosol data, Nature, 355, 626–628, https://doi.org/10.1038/355626a0, 1992.

Watanabe, S. and Kawatani, Y.: Sensitivity of the QBO to mean tropical upwelling under a changing climate simulated with an Earth System Model, Journal of the Meteorological Society of Japan, Series II, 90A, 351–360, https://doi.org/10.2151/jmsj.2012-A20, 2012.

Yoo, C. and Son, S.-W.: Modulation of the boreal wintertime Madden-Julian oscillation by the stratospheric quasi-biennial oscillation, Geophys. Res. Lett., 43, 1392–1398, https://doi.org/10.1002%2F2016GL067762, 2016.

Zawodny, J. M. and McCormick, M. P.: Stratospheric Aerosol and Gas Experiment II measurements of the quasi-biennial oscilla- tions in ozone and nitrogen dioxide, J. Geophys. Res., 96, 9371– 9377, http://dx.doi.org/10.1029/91JD00517, 1991.

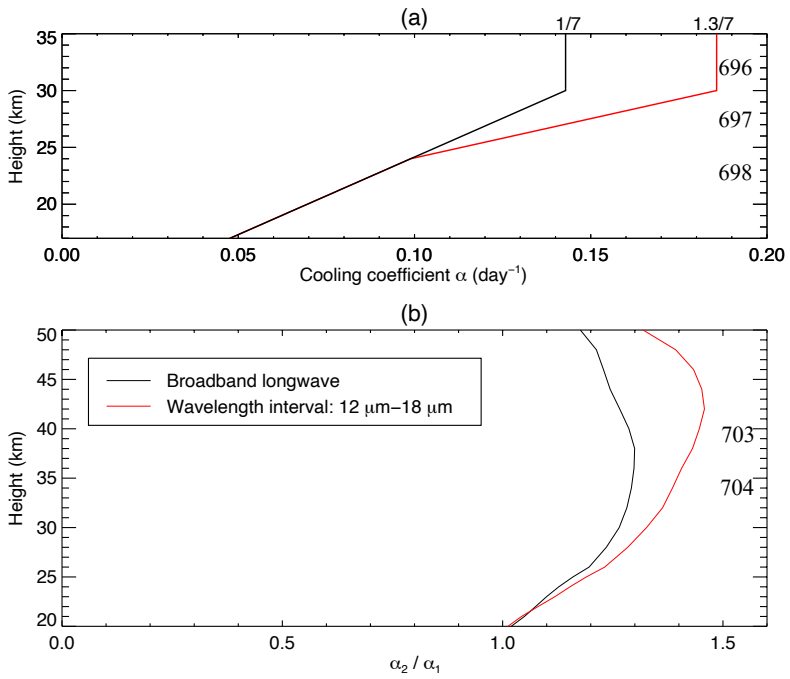

FIG. 1: (a) Profiles of Newtonian cooling coefficients: The smaller values (black line) are used for the control runs while the larger values (red line) are used for the experimental runs. (b) Profiles of the ratio of α_2 to α_1, where α_1 and α_2 denote the Newtonian cooling coefficient for the reference CO_2 and the doubled CO_2, respectively. The black line depicts the ratio for the broadband longwave ($5\ \mu m - 100\ \mu m$) and the red line delineates that for the CO_2 absorption band ($12\ \mu m - 18\ \mu m$).

Deleted: profiles

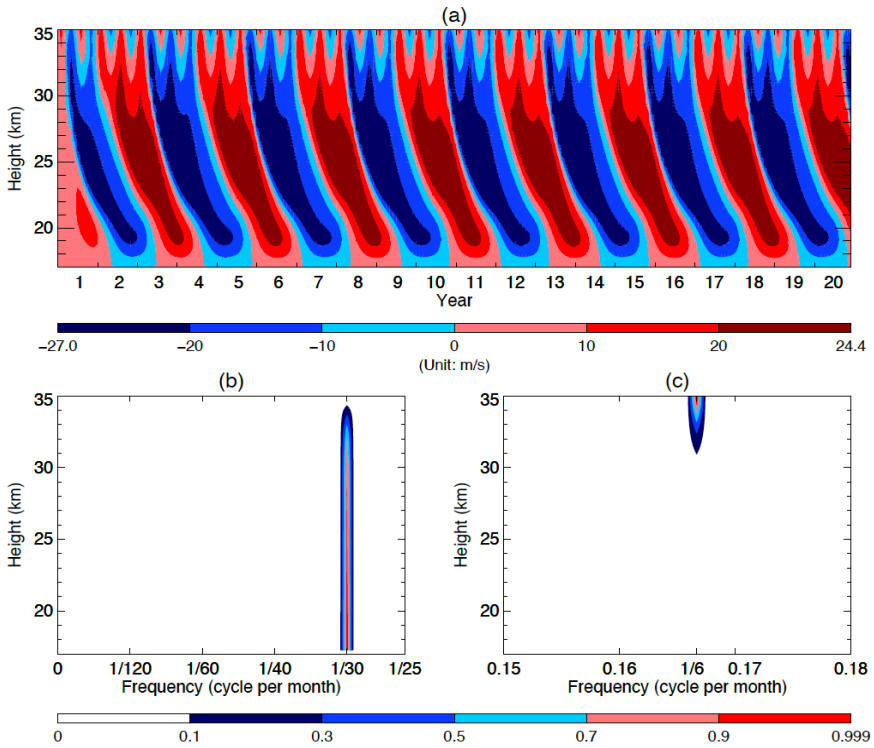

FIG. 2: (a) Time–height section of the monthly averaged mean zonal wind over the first 20 years from the HL's original model. (b) and (c) Frequency–height section of the power spectral densities (PSD) of the standardized monthly averaged mean zonal wind of the 100 years. Note that in order to better visualize the PSD in (b) and (c), we trimmed off the blank segments for the frequencies ranging from $\frac{1}{25}$ to 0.15 cycle per month and those ranging from 0.18 to 0.5 cycle per month.

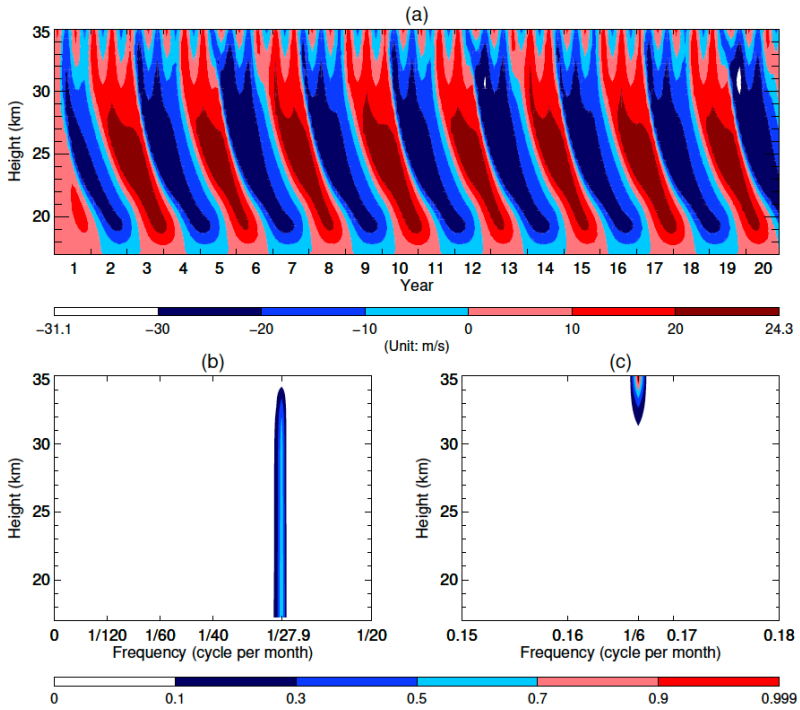

FIG. 3: (a) Same as FIG. 2a, but with the enhanced $\alpha(z)$ depicted as the red line in FIG. 1a. (b) and (c) Frequency–height section of the power spectral densities (PSD) of the standardized monthly averaged mean zonal wind of the 100 years. Note that in order to better visualize the PSD in (b) and (c), we trimmed off the blank segments for the frequencies ranging from $\frac{1}{20}$ to 0.15 cycle per month and those ranging from 0.18 to 0.5 cycle per month.

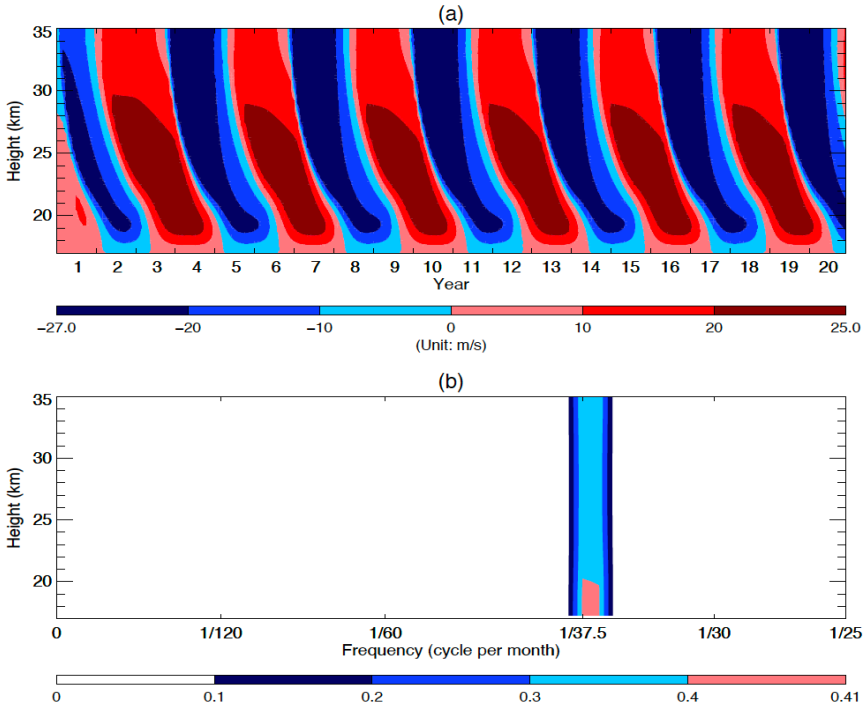

FIG. 4: (a) Time–height section of the monthly averaged mean zonal wind over the first 20 years from the HL's model without the semiannual forcing. (b) Frequency–height section of the power spectral densities (PSD) of the standardized monthly averaged mean zonal wind of the 100 years. Note that in order to visualize the PSD, we trimmed off the blank segment for the frequencies ranging from $\frac{1}{25}$ to 0.5 cycle per month.

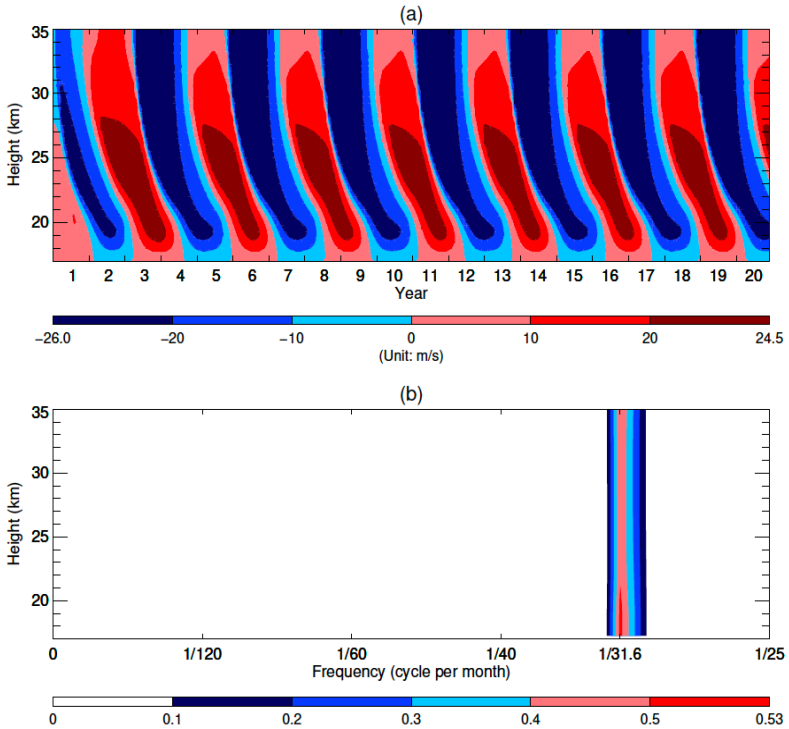

FIG. 5: (a) Same as FIG. 4a, but with the enhanced $\alpha(z)$ depicted as the red line in FIG. 1a. (b) Same as FIG. 4b, but for the doubled CO_2 Run.

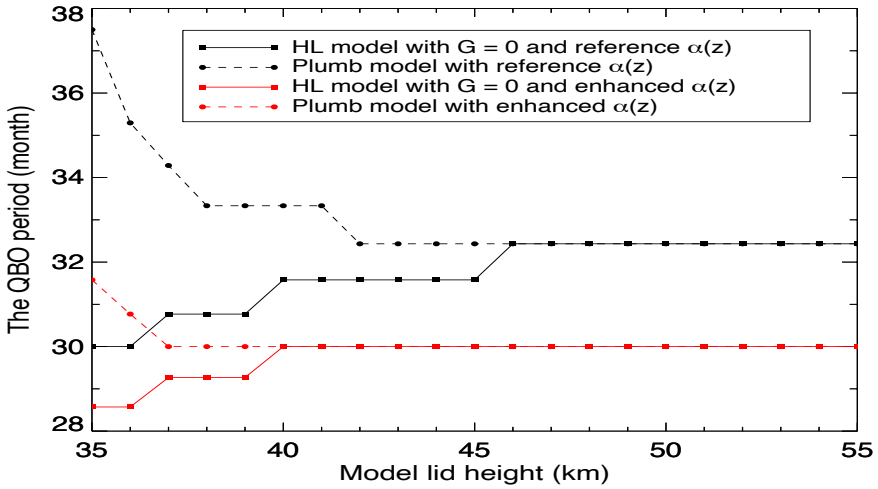

FIG. 6: The relationship between the simulated QBO period with the height of the model lid. Black and red lines depict the results from using the reference radiative damping and the enhanced radiative damping respectively while solid and dashed lines delineate the results from the HL model with $G = 0$ and the Plumb model respectively.